Acta Geotechnica (2021) 16:2071–2088
https://doi.org/10.1007/s11440-021-01143-7

RESEARCH PAPER

Influence of particle size on the drained shear behavior of a dense fluvial sand

Yibing Deng[1] · Yuksel Yilmaz[2] · Aydin Gokce[2] · Ching S. Chang[1]

Received: 25 August 2020 / Accepted: 8 January 2021 / Published online: 29 January 2021

Abstract
Particle morphology, including particle shape and particle size, has significant influence on the shear behavior of granular soils. The effect of particle shape has been investigated in several studies. However, the effect of particle size has not yet been paid much attention. In this study, the effect of particle size on the shear strength and the stress–dilatancy behavior of sands was assessed through a series of drained triaxial compression tests on dense uniform silica sands. The effect of particle size was analyzed on various aspects of mechanical behavior: the stress–strain response, the shear band formation, the peak-stress axial strain, the peak dilation angle, the peak friction angle, the critical-state friction angle, and the stress–dilatancy relations. Furthermore, we noticed that the particle shape of silica sands usually varies with particle size. The effect of this morphologic characteristic on mechanical behavior was also discussed by comparing the experimental results on silica sands with those reported on glass beads and Péribonka sand (Harehdasht et al. in Int J Geomech 17:04017077, 2017). The results show that particle size significantly influences the peak friction angle, the peak dilation angle and the stress–dilatancy behavior. The underlying mechanism for the effect of particle size was discussed from the perspective of kinematic movement at particle level.

Keywords Dilatancy · Drained triaxial test · Particle size · Sands · Shear strength

1 Introduction

The shear behavior of granular soils is an important topic in soil mechanics and geotechnical engineering. One distinctive feature of the shear behavior is dilatancy, which plays a key role in controlling the shear strength. Rowe [2] pioneeringly developed the stress–dilatancy relation by applying the principle of energy minimization. Afterward, De Josselin De Jong [3] proved that Rowe's stress–dilatancy relation is valid. Rowe's stress–dilatancy relation has been extensively used in describing the shear behavior of granular materials [4–7].

The stress–dilatancy behavior is affected by many factors: external conditions (density, confining stress, strain history, etc.) [2, 5, 8–11], and particle morphology (gradation, size, shape (measured by roundness, angularity, aspect ratio, sphericity, etc.), surface roughness and mineralogy) [1, 12–16].

About the external conditions, the stress–dilatancy relation proposed by Rowe [2] cannot capture these dependencies. To overcome these limitations, Wan and Guo [6] modified Rowe's stress–dilatancy relation in a phenomenological way to account for some of these dependencies by the introduction of a void ratio factor. Bolton [17] proposed an empirical equation to quantify the influences of the density and confining pressure on peak friction angle (ϕ_p) and dilation angle (ψ_p). Both the modified Rowe's stress–dilatancy relation and Bolton's equation introduced the critical state friction angle (ϕ_{cv}) to

✉ Ching S. Chang
cchang@engin.umass.edu

Yibing Deng
yibingdeng@engin.umass.edu

Yuksel Yilmaz
yyuksel@gazi.edu.tr

Aydin Gokce
agokce@gazi.edu.tr

[1] Department of Civil and Environmental Engineering, University of Massachusetts Amherst, Amherst, MA, USA

[2] Department of Civil Engineering, Gazi University, Ankara, Turkey

establish the relation between mobilized friction angle and dilation angle.

Among the particle morphology factors, particle size and particle roundness are two most important intrinsic geometric properties that affect the shear behavior of granular soils. Researchers are often interested in the influence of particle size and particle roundness on the stress–dilatancy behavior of granular soils (i.e., critical state friction angle ϕ_{cv}, and stress–dilatancy related parameters such as peak friction angle ϕ_p, and peak dilation angle ψ_p). Many experimental research works have been devoted to particle shape, for example in the critical state friction angle [12, 13, 18–20], in peak friction and dilation angles [6, 12, 13, 15, 21–23], and in stress–dilatancy relation [1, 13, 15].

On the other hand, for the effect of particle size, the works are scarce. The available research works are summarized on the following three properties:

(1) *critical state friction angle*: For critical state friction angle, particle size has no effect as advocated from a discrete element analysis of round particles [24–26], and supported from experiments on glass beads and Péribonka sand [1].

(2) *peak friction and dilation angles*: About particle size effect on peak shear strength of crushable soil, studied can be found on shear strength of rockfill [27, 28]. For non-crushable silica sand, on the other hand, the experimental studies are scarce. The triaxial test experiments of glass beads and Péribonka sand [1] indicated that the particle size has a significant influence on both peak friction and dilation angles. The assembly of small particles evidently show higher peak friction and dilation angles than that of the assembly of large particles for glass beads and Péribonka sand.

(3) *stress–dilatancy relation*: Harehdasht et al. [1] showed that there is a significant particle size effect on the parameters of modified Rowe's equation and of Bolton's equation for glass beads and Péribonka sand.

Overall, the results reported in the literature have shown significant effect of particle size on peak friction angle ϕ_p and on peak dilation angle ψ_p. However, the results are based on limited experimental studies on Péribonka sand and on glass beads. Thus, it is desirable to have more tests on a different type of sand to confirm the significance of size effect on sand.

For this purpose, we selected Pasabahce silica sand, obtained from the strait of Istanbul, which has an average roundness of 0.25 compared to 0.44 of Péribonka sand. The sand was sieved into seven size groups of uniform sand. A series of drained triaxial compression tests at various confining pressures were conducted on the dense uniform silica sands with various particle sizes.

The test results due to the effect of particle size are analyzed on various aspects of mechanical behavior: the stress–strain response, the shear band formation, the peak-stress axial strain, the peak dilation angle and the peak friction angle, the critical-state friction angle and the stress–dilatancy relations. In some aspects, the measured behavior is very different by comparing the results with those of glass beads and Péribonka sand [1]. The specific feature of the measured stress–dilatancy behavior will be discussed.

2 Materials and testing program

2.1 Material and its physical properties

Pasabahce silica sand (herein referred to as silica sand) is formed as a result of disintegration of magmatic metamorphic rocks being rich in quartz. The fluvial transportation brought it to actual deposit in Istanbul, Turkey. This silica sand was used in this experimental study. Samples were prepared by the following 7 grades of "uniform" sands: No.16-No.18, No.18-No.30, No.30-No.50, No.50-No.80, No.80-No.100, No.100-No.120, No.120-No.200. Each uniform sand is named by the upper sieve number and the lower sieve number. The particle sizes and specific gravities of these seven uniform sands are listed in Table 1. A qualitative look at the shape and surface texture of the individual sand grains is shown in Fig. 1, which reveals that the sand grains are mostly subangular.

In soil mechanics and engineering geology fields, roundness is the most commonly used measure for quantification of particle shape characteristics. Roundness (R_W), as defined by Wadell [29], is the ratio of the average radius

Table 1 Properties of the uniform silica sands of seven different particle sizes

Uniform sand*	d_{50} (mm)	e_{max}	e_{min}	Roundness	G_s
#16-#18	1.086	0.901	0.632	0.36	2.624
#18-#30	0.775	0.907	0.64	0.35	2.625
#30-#50	0.424	0.999	0.698	0.26	2.64
#50-#80	0.232	1.102	0.786	0.17	2.646
#80-#100	0.164	1.128	0.768	0.19	2.654
#100-#120	0.137	1.108	0.778	0.18	2.652
#120-#200	0.096	1.099	0.717	0.23	2.654

*the uniform silica sand is artificially graded using two adjacent sieves. # No.- # No. is the upper sieve number and the lower sieve number, respectively, for a uniform sand

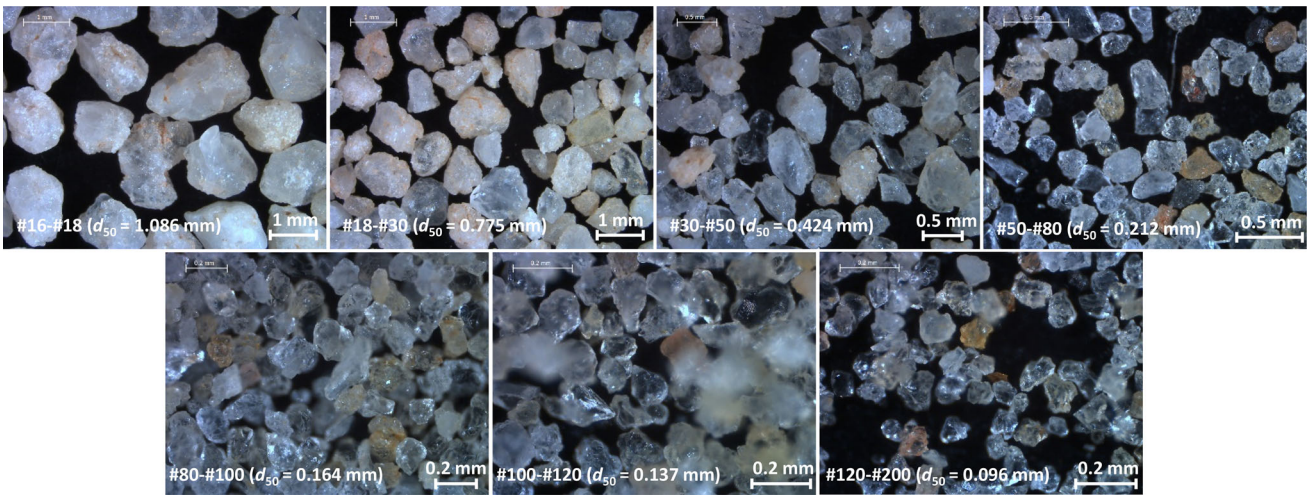

Fig. 1 Micrographs for Pasabahce silica sand of different particle sizes

of curvature of the particle edges to the radius of the maximum inscribed circle:

$$R_{\mathrm{W}} = \frac{\frac{1}{n}\sum_{i=1}^{n} r_{\mathrm{i}}}{r_{\mathrm{ins}}} \tag{1}$$

where n is the total number of corners, r_i is the radius of circle fitting the i-th corner, and r_{ins} is the radius of inscribed circle as shown in Fig. 2. A corner for a sand particle was defined by the following procedure: a two-dimensional projected image of the particle was obtained by using a microscope. Then, the outline of the particle was traced. Each corner along the outline was readily identified using intuition and fitted with a circle. For each uniform sand sample, approximately 50 sand particles were selected to determine the roundness using Eq. (1). The calculated roundness for uniform sand samples of seven size-classes are listed in Table 1.

The minimum void ratio (maximum index density) and the maximum void ratio (minimum index density) of the sand samples were determined according to Method 2A of ASTM D4253 [30] and Method B of ASTM D4254 [31], respectively. The minimum and the maximum void ratios of samples are tabulated in Table 1.

2.2 Experimental program

A conventional triaxial test apparatus was used to study the drained shear behavior of the seven uniform sands. Each test was performed under 3 confining pressures, i.e., 100, 200 and 400 kPa. A total number of 21 drained triaxial compression tests were performed using the conventional triaxial test apparatus on cylindrical specimens (50 mm in diameter and 100 mm in height).

Since our aim is to study stress–dilatancy behavior of the samples compacted at very dense condition, wet compaction is preferred to dry compaction for preparing the samples. Thus, we prepared the samples by wet compaction (total five layers for each sample).

Note that the minimum and the maximum void ratios of the samples were obtained by using dry sand (according to ASTM D4253 [30] and ASTM D4254 [31]). The initial void ratios e_0 of all samples after preparation using wet compaction are plotted in Fig. 3, compared with the

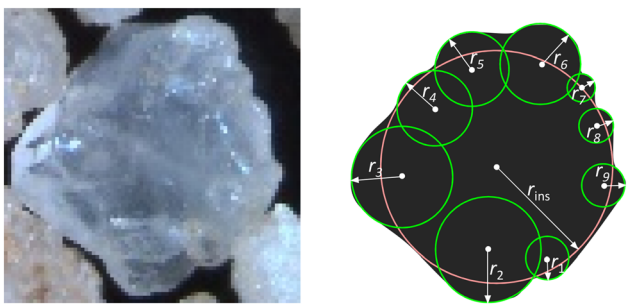

Fig. 2 Determination of particle roundness

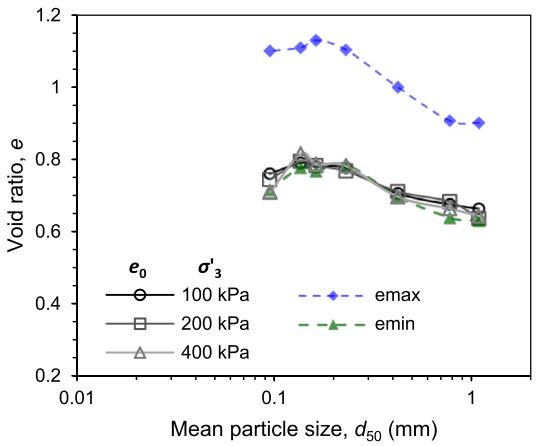

Fig. 3 The initial void ratios e_0 of all silica sand samples

measured values of e_{min} and e_{max}. As shown in Fig. 3, the value of e_0 for all samples is nearly the same as that of e_{min}, which indicates that all samples have initial relative density I_d of around 95%.

The procedures of the drained triaxial compression test consisted of three steps. First, pouring and tamping predetermined sand mass into the cell so that a series of dense samples were prepared to similar relative densities. The initial void ratios of each sample are listed in Table 2. Then, the prepared sample was consolidated under a given confining stress. After consolidation, the sample was sheared until failure by compressing the sample with a constant vertical displacement rate of 0.2 mm/min. During the course of shearing, the sample was allowed to drain. The drained triaxial compression tests for each sample were performed under three different effective confining stresses of 100 kPa, 200 kPa, and 400 kPa. Particle breakage was not observed in all tests. The results of the triaxial tests are summarized in Table 2.

In this paper, major and minor principal effective stresses are denoted by $\sigma_1^{'}$ and $\sigma_3^{'}$. Axial and volumetric strains are denoted by ε_a and ε_v. Contractive strains are considered as positive and dilative strains are considered as negative.

3 Test results

3.1 Stress–strain and volume change responses

Figure 4 shows deviatoric stress q (i.e., $q = \sigma_1^{'} - \sigma_3^{'}$) and volumetric strain (ε_v) versus axial strain (ε_a) relationships for the 7 uniform sands under three different confining stresses (100, 200, 400 kPa). As shown in Fig. 4, all samples after peak exhibit softening behavior in the stress–strain curves, and exhibit dilative behavior in the volumetric strain curves. Following the initial slight contraction at a small axial strain, dilation then commences. The dilation continues during shearing until the deviatoric stress q mobilizes to the peak value. After the peak deviatoric stress, the stress decreases and approaches to a stable value, and the sample reaches to the critical state.

The effect of sample variability on the stress–strain curves in Fig. 4 is carefully evaluated by repeating several

Table 2 Summary results of drained triaxial compression tests on uniform silica sand samples

Uniform sand	Void ratio					Shearing					
	Initial	Consolidation	onset of dilatancy	peak stress	critical state	confining stress	strain at peak stress		Friction angle at onset of dilatancy	Peak friction angle	Peak. dilation angle
							Axial	Volumetric			
	e_0	e_c	e_f	e_p	e_{cs}	σ'_3 (kPa)	ε_a (%)	ε_v (%)	ϕ_f (°)	ϕ_p (°)	ψ_p (°)
#16-#18	0.664	0.656	0.653	0.699	0.761	100	6.8	−2.6	26.0	37.6	11.4
	0.637	0.621	0.617	0.663	0.719	200	9.5	−2.6	28.6	38.0	10.9
	0.644	0.614	0.608	0.641	0.697	400	11.8	−1.7	29.6	37.5	9.1
#18-#30	0.676	0.668	0.665	0.709	0.771	100	7.3	−2.4	27.2	37.2	10.1
	0.683	0.667	0.663	0.701	0.741	200	8.0	−2.1	28.2	37.6	10.1
	0.664	0.638	0.633	0.668	0.711	400	12.0	−1.9	29.2	36.8	7.7
#30-#50	0.706	0.701	0.698	0.753	0.824	100	7.2	−3.1	25.4	38.7	13.3
	0.711	0.700	0.696	0.746	0.789	200	9.4	−2.7	28.2	39.0	11.7
	0.697	0.677	0.671	0.706	0.755	400	11.3	−1.7	30.3	38.3	8.9
#50-#80	0.776	0.771	0.768	0.825	0.892	100	7.3	−3.1	28.1	40.4	13.8
	0.767	0.756	0.752	0.812	0.876	200	9.2	−3.2	29.2	40.0	12.3
	0.782	0.762	0.754	0.797	0.851	400	12.0	−2.0	31.0	38.9	10.3
#80-#100	0.779	0.775	0.773	0.832	0.886	100	6.5	−3.2	27.1	42.1	16.1
	0.782	0.771	0.766	0.808	0.861	200	8.6	−2.1	30.2	39.3	11.5
	0.787	0.769	0.763	0.801	0.838	400	9.4	−1.8	32.1	40.3	11.5
#100-#120	0.79	0.787	0.785	0.843	0.889	100	6.5	−3.1	29.8	43.4	17.1
	0.794	0.784	0.780	0.829	0.870	200	7.8	−2.0	30.3	39.9	12.6
	0.815	0.797	0.791	0.822	0.847	400	10.3	−1.4	30.9	38.6	9.1
#120-#200	0.76	0.755	0.753	0.787	0.831	100	4.9	−1.8	29.0	40.3	15.8
	0.744	0.734	0.730	0.770	0.796	200	7.0	−2.1	30.6	41.1	13.3
	0.710	0.695	0.690	0.735	0.764	400	10.8	−2.4	29.7	39.7	11.3

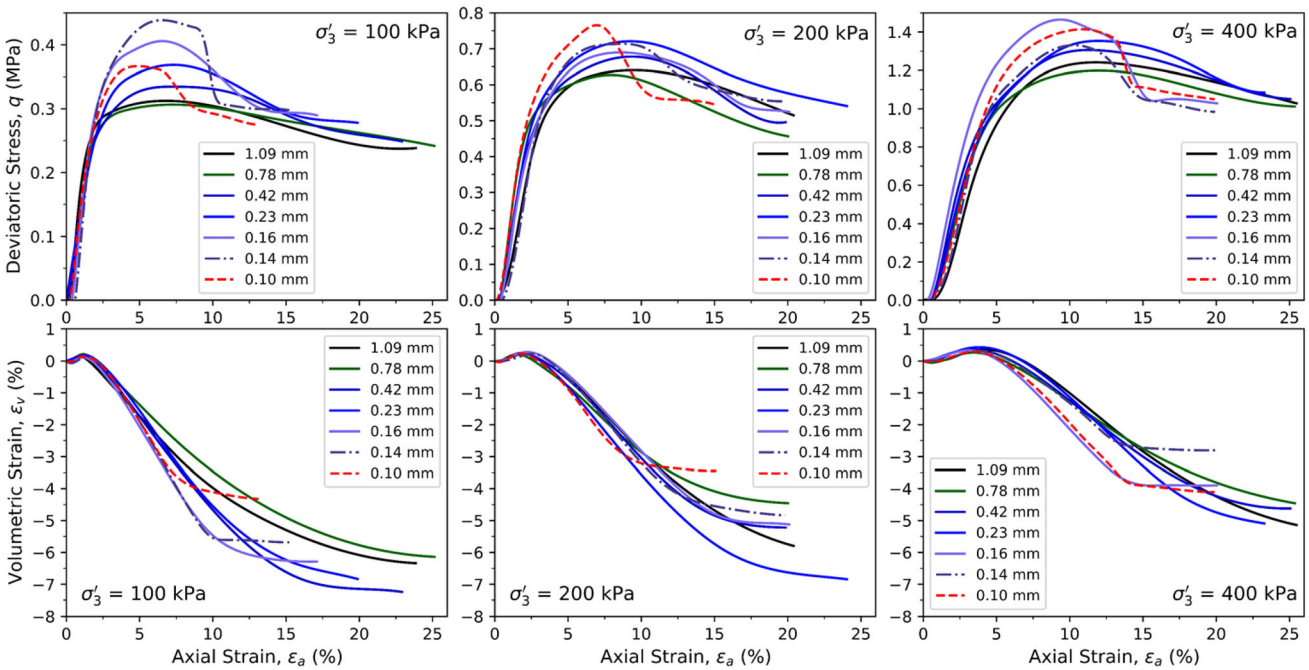

Fig. 4 Stress–strain curves of the drained triaxial compression tests on uniform sand samples of various particle sizes

tests under the same testing conditions. A set of typical repeated tests for the uniform sand #50-#80 with a confining pressure of 200 kPa is shown in Appendix A. The variability of the stress–strain curves is small as shown in Fig. 24. In Appendix A, the effect of sample variability on various interpreted mechanical properties is found to be reasonably small and would not affect the conclusion of this study.

The effect of confining stress on the stress–strain behavior and dilation can be observed by comparing the test results of the three different confining stresses in Fig. 4. An increase in the confining stress leads to an increase in the deviatoric stress and a decrease in dilation. In addition, both the onset of dilation and reaching to peak stress require more axial strain under a higher confining stress.

As shown in Fig. 4, peak deviatoric stress and dilation are affected by the particle size of specimen. In general, the specimen with smaller particles tends to have higher peak deviatoric stress and higher dilation. The effect of particle size on strength and dilation will be discussed in the later section.

It is noted that for some specimen with small particle size (e.g., d_{50} = 0.14 and 0.1 mm) in Fig. 4, the deviatoric stress decreases rapidly after the peak value, then approaches to a stable value. The rapid decrease in the deviatoric stress was expected to be caused by the occurrence of shear band, which will be discussed later.

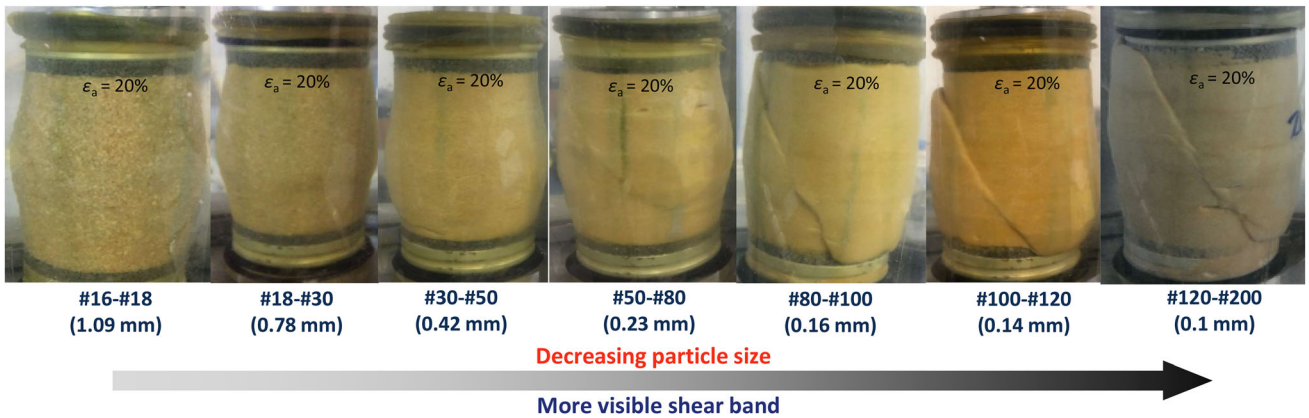

Fig. 5 The failure patterns for samples of various particle sizes at 20% axial strain under the confining stress of 400 kPa. (Large particle samples: #16-#18, #18-#30, and #30-#50; small particle samples: #50-#80, #80-#100, #100-#120, and #120-#200)

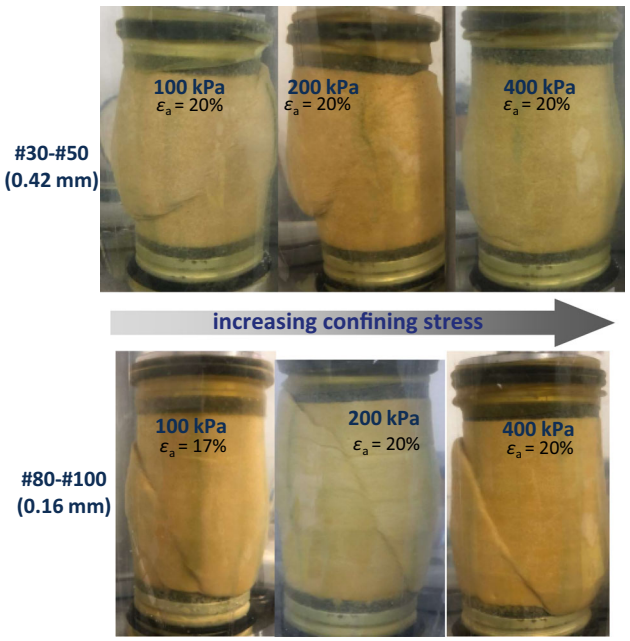

Fig. 6 The failure patterns for samples of two different particle sizes at large strain (about 20%) under different confining stresses

3.2 Shear band

Shear bands were observed in some samples during shearing. It was found that particle size and confining pressure have influence on the formation of shear band.

Compared to large particle samples, the smaller particle samples are more likely to have visible shear band formations. As shown in Fig. 5 at large axial strain (e.g., ε_a = 20%), the larger particle samples (1.09 mm, 0.78 mm and 0.42 mm) did not have visible shear bands, while for the smaller particle samples (0.23 mm, 0.16 mm, 0.14 mm and 0.1 mm), the evidences of shear bands are obvious at the 20% axial strain level. In other studies on shear band, similar phenomenon was also found that the shear band occurs at lower axial strain and the band width is narrower for small-particle samples [32–34].

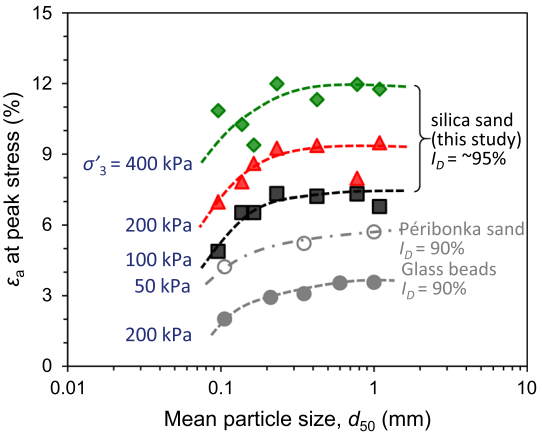

Fig. 7 The axial strain at peak stress versus particle size for samples under three different confining stresses (the data of glass beads were extracted from Harehdasht et al. [1])

The experimental results show that confining stress suppresses the occurrence of shear band. As shown in Fig. 6, for large particle samples (#30-#50), the shear band occurs for confining stress 100 kPa, but not for 400 kPa. For small particle samples (#80-#100), shear band occurs at 17% axial strain for confining stress 100 kPa, whereas it occurs at 20% axial strain for confining stress 400 kPa.

3.3 Axial strain at peak stress

Figure 7 shows the axial strain at peak deviatoric stress versus particle size for three confining stresses. Evident effects of particle size and confining stress were observed.

To compare with our results, we extracted the data of round glass beads and Péribonka sand of various sizes from Harehdasht et al. [1]. These data are also plotted in Fig. 7. As shown in Fig. 7, for uniform silica sand, the sample with larger particle size requires a larger axial strain to reach the peak stress. This general trend is consistent with the results of uniform glass beads and Péribonka sand. The axial strain at the peak stress is significantly lower for glass beads than that of silica sand. This may be caused by the difference in surface roughness and the roundness of particles [1, 12].

It is noted that the axial strain, corresponding to peak stress, is less than 12% for all test samples. However, for all test samples, the shear band occurrence become visible after axial strain is beyond 20% as shown in Fig. 5. Therefore, at peak stress state, the shear band formation is just at the beginning of forming stage, and the sample is relatively in a uniform strain condition.

For a given particle size, the higher the confining stress, the larger strain the sample requires to reach the peak stress. This trend is consistent with experimental results of uniform sand commonly reported in the literature.

4 Analyses of measured results of ϕ_p, $\overline{\phi}_{fp}$,ψ_p and ϕ_{cv}

4.1 Stress–dilatancy relation

The stress–dilatancy relations are plotted in Fig. 8 for seven uniform sands under three confining stresses. Prior to the peak dilation, all stress–dilatancy relations show a consistent increase in the stress ratio $R = \sigma'_1/\sigma'_3$ with the dilatancy factor $D = 1 - d\varepsilon_v/d\varepsilon_a$. Once D reaches a peak, the curves naturally reverse, giving a "hook" in the curve as D drops to the critical state. It was found that D_{max} and

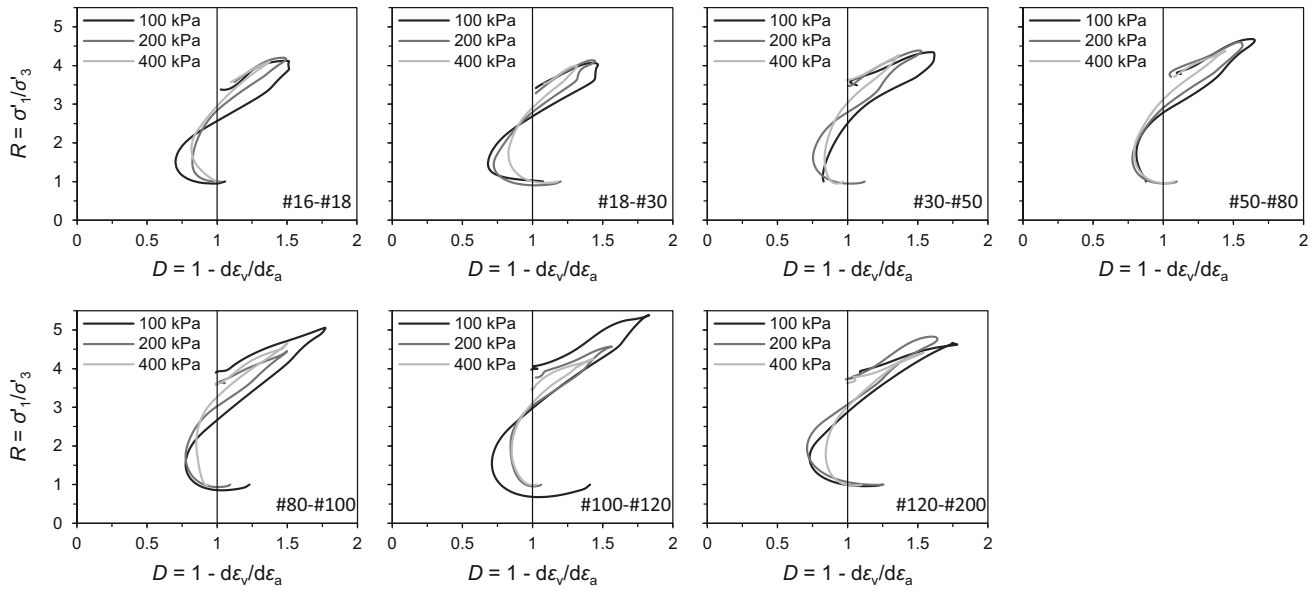

Fig. 8 The stress–dilatancy relations for samples of various particle sizes under three different confining stresses

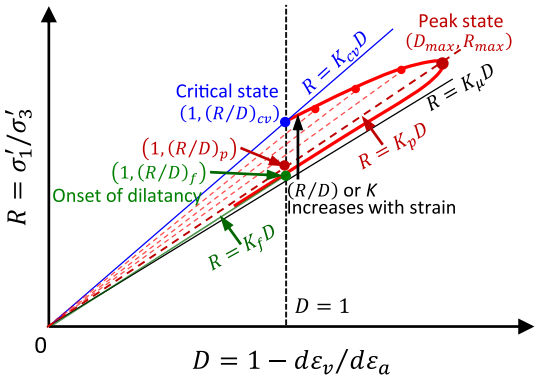

Fig. 9 A schematic plot of stress–dilatancy relation

the corresponding R_{max} on a stress–dilatancy relation decrease with an increase in confining stress and decrease with an increase in particle size, which is consistent with results of round glass beads reported by Harehdasht et al. [1]. The value of R when $D = 1$ (i.e., onset of dilatancy) rises with an increase in confining stress for each particle size.

Based on Fig. 8, a typical stress–dilatancy relation is given in the schematic Fig. 9. The ratio R/D increases with deformation from the ratio $(R/D)_{\mathrm{f}}$ at the onset of dilatancy to the ratio $(R/D)_{\mathrm{cv}}$ at critical state. The ratio $(R/D)_{\mathrm{p}}$ at peak state is near to the ratio $(R/D)_{\mathrm{f}}$. Both of $(R/D)_{\mathrm{p}}$ and $(R/D)_{\mathrm{f}}$ are functions of confining stress and current void ratio [6].

Rowe's stress–dilatancy theory is used to analyze the test results. According to [2], the stress–dilatancy relation is given by

$$R = K\left(1 - \frac{d\varepsilon_v}{d\varepsilon_a}\right) = KD; \text{where } K = \tan^2\left(\pi/4 + \overline{\phi}_f/2\right) \tag{2}$$

where K (= R/D) is a material constant. The angle $\overline{\phi}_f$ refers to an equivalent friction angle which reflects the influence of sliding, rolling and rearrangement of particles. In Fig. 9, Eq. (2) represents a straight line connecting a point on the stress–dilatancy plot and the coordinate origin. All data of R versus D are located between the line of $R = K_{cv}D$ and the line of $R = K_{\mu}D$. Herein, K_{cv} and K_{μ} correspond to the critical state friction angel ϕ_{cv} and the inter-particle friction angle ϕ_{μ}, respectively. Note that, $\overline{\phi}_f$ is not a constant, which varies between ϕ_{μ} and ϕ_{cv} with deformation history and density [2, 6]. In the pre-peak stage (i.e., hardening stage), variation of $\overline{\phi}_f$ is small. In the post-peak stage (i.e., softening stage), variation of $\overline{\phi}_f$ is large.

An alternative form of Rowe's equation (Eq. 2) can be derived by introducing a mobilized Coulomb friction angle ϕ_m, defined as $\sin\phi_m = \left(\sigma_1' - \sigma_3'\right)/\left(\sigma_1' + \sigma_3'\right)$, and invoking a dilation angle ψ defined by Vermeer and de Borst [35] (see Appendix B). Rowe's equation can then be expressed in the following alternative form

$$sin\psi = \frac{sin\phi_m - \sin\overline{\phi}_f}{1 - sin\phi_m \sin\overline{\phi}_f} \tag{3}$$

4.2 Determination of friction and dilation angles

(1) *Peak friction angle ϕ_p and peak dilation angle ψ_p.*

As shown in Fig. 9 for a triaxial test, the peak point on the stress–dilatancy curve can be identified and then the corresponding set of R_{max} and D_{max} can be found. This point generally coincides with the maximum deviatoric stress in the stress-axial strain curve shown in Fig. 4. The peak friction angle ϕ_p was calculated from the value of R_{max} based on the definition of mobilized Coulomb friction angle. The peak dilation angle ψ_p was calculated from the value of D_{max} based on the definition of dilation angle defined by Vermeer and de Borst [35] (i.e., Eq. (11) in Appendix B). The obtained values of ϕ_p and ψ_p for the 21 tests are listed in Table 2.

(2) *The friction angle at the onset of dilation ϕ_f and the equivalent friction angle at peak state $\overline{\phi}_{fp}$.*

The mobilized Coulomb friction angle at the onset of dilation ϕ_f is corresponding to the value K_f in the stress–dilatancy relation (Fig. 9). The obtained values of ϕ_f for the 21 tests are listed in Table 2. The equivalent peak friction angle, denoted by $\overline{\phi}_{fp}$, is corresponding to the value K_p in the stress–dilatancy relation (Fig. 9). The value of $\overline{\phi}_{fp}$ is near to that of ϕ_f. Frequently, K_p is considered to be same as K_f in the range of R prior to and nearly up to the peak value, which is supported by experimental data presented by Rowe [2] and others [15, 36].

(3) *The friction angle at critical state ϕ_{cv}.*

The critical state friction angle ϕ_{cv} is mobilized at large strain when the sample is sheared at a constant volume. The value of ϕ_{cv} is independent on initial density and confining pressure [37]. According to the suggestion by Nova [38], stress ratio q/p' and dilatancy ratio $d\varepsilon_v^p/d\varepsilon_q^p$ have the following relationship:

$$\frac{d\varepsilon_{\mathrm{v}}^{\mathrm{p}}}{d\varepsilon_{\mathrm{q}}^{\mathrm{p}}} = (M - \frac{q}{p'})/(1 - N) \tag{4}$$

where M, N, p' and ε_q are the critical state stress ratio, volumetric coupling coefficient, mean effective stress, and deviatoric strain, respectively. The superscript 'p' stands for plastic. $p' = (\sigma_1' + 2\sigma_3')/3$ and $\varepsilon_q = \varepsilon_a - \varepsilon_v/3$.

At post-peak stress, $d\varepsilon_v^p/d\varepsilon_q^p \approx d\varepsilon_v/d\varepsilon_q$ since the magnitude of elastic strain is negligible. All tests for a given soil in the post-peak stage can be represented by Eq. (4) using the critical state stress ratio M and volumetric coupling coefficient N. The optimal critical state $\overline{M}$ for each uniform sand can be calculated by the following minimization:

$$\overline{M} = \underset{M,N}{\operatorname{argmin}} \left[\sum_{i=1}^{T_n} \sum_{j=1}^{n} \left((1 - N) \cdot \frac{d\varepsilon_v}{d\varepsilon_q} + \frac{q}{p'} - M \right)^2 \right] \tag{5}$$

where T_n is the number of tests for each uniform sand (T_n = 3 for this study, i.e., three different confining stresses); and n is the number of points evaluated along each stress path (with equal $\Delta\varepsilon_a = 0.1\%$ intervals, from the peak stress up to the end of the test).

The corresponding critical state friction angle ϕ_{cv} can be obtained from

$$sin\phi_{cv} = \frac{3\overline{M}}{6 + \overline{M}} \tag{6}$$

The obtained ϕ_{cv} are listed in Table 3.

Table 3 The determined ϕ_{cv} for the uniform silica sands of seven different particle sizes

Uniform sand	#16-#18	#18-#30	#30-#50	#50-#80	#80-#100	#100-#120	#120-#200
ϕ_{cv} ( )	32.4	32.7	34.2	34.8	35.1	35.2	35.3

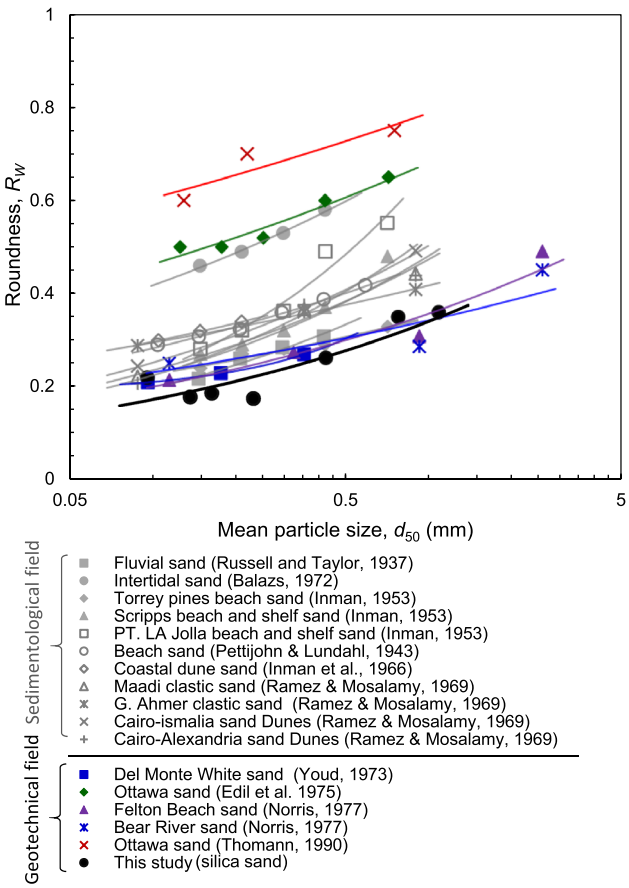

Fig. 10 Size-roundness correlation for natural sands

5 Discussion of test results of ϕ_p, $\overline{\phi}_{fp}$,ψ_p

Herein, we are interested to investigate the influence of particle size and particle roundness on the measured peak friction angle, equivalent peak friction angle and dilation angle for silica sand. The experimental results of silica sand will be compared with those of round glass beads and Péribonka sand.

When the particle size and particle roundness are two independent variables (i.e., uncorrelated), their effect can be evaluated using multi-variable regression analysis. However, if the two variables are strongly correlated, then the regression analysis cannot attain a stable solution due to a notorious problem called "multi-linearity," thus it is not feasible to separate the influence of each variable. Interestingly, such problem occurs for the Pasabahce silica sand.

5.1 Size-roundness correlation of fluvial sand

Pasabahce silica sand, from the view of geological origin, is a fluvial transport sand. Studies in sedimentology have shown that the size-roundness correlation is strong for sands with same genesis and transport history (shown in Fig. 10) [39–44]. The larger size particles of this type of sand are much better rounded than the smaller grades. This morphologic characteristic was also observed in geotechnical investigations [45–49]. The measured roundness for the silica sand used in this study confirms its strong correlation with particle size (see Fig. 10). The data points of Pasabahce silica sand is among the group of fluvial sands or beach sands.

Because of this special feature, it is difficult to change one variable by keeping another constant. The roundness and size tend to change in unison. Thus, the measured mechanical properties plotted against particle size do not reflect the effect of particle size alone, and rather, it includes the joined effects of particle roundness and particle size. Thus, this strong correlation makes it unfeasible to determine the role of each variable for fluvial sand.

In order to assess the influence of size and roundness for fluvial sand, it is not only necessary to investigate separately the relationship between mechanical properties versus particle size, and the relationship between mechanical properties versus particle roundness, but also needed to compare these effects with other type of materials such as glass beads and Péribonka sand, which do not have correlation between size and roundness.

5.2 Peak friction and dilation angles

5.2.1 Influence of particle size

Figure 11 shows the values of ϕ_p and $\overline{\phi}_{fp}$, versus particle size for various confining stresses for silica sand. For comparison, the values of ϕ_p and $\overline{\phi}_{fp}$ for glass beads and Péribonka sand are also plotted. For all three materials, the values of ϕ_p decrease substantially with an increase in particle size. The values of $\overline{\phi}_{fp}$, however, are nearly independent of particle size for both silica and Péribonka sand, and show small variation with respect to particle size for glass beads.

Figure 12 shows that the value of ψ_p decreases significantly with an increase in particle size for silica sand. The results, extracted from the data of glass beads and Péribonka sand [1], also show the same trend.

Both Fig. 11 and Fig. 12 evidently show significant influence of particle size on peak friction and dilation angles.

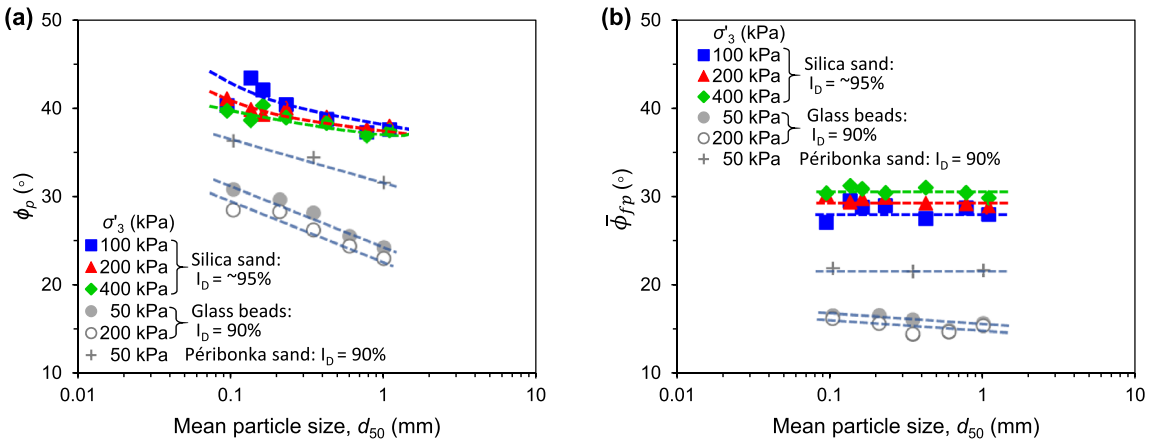

Fig. 11 Influence of particle size and confining stress on peak friction angle ϕ_p and equivalent peak friction angle $\overline{\phi}_{fp}$ for silica sand, glass beads, and Péribonka sand

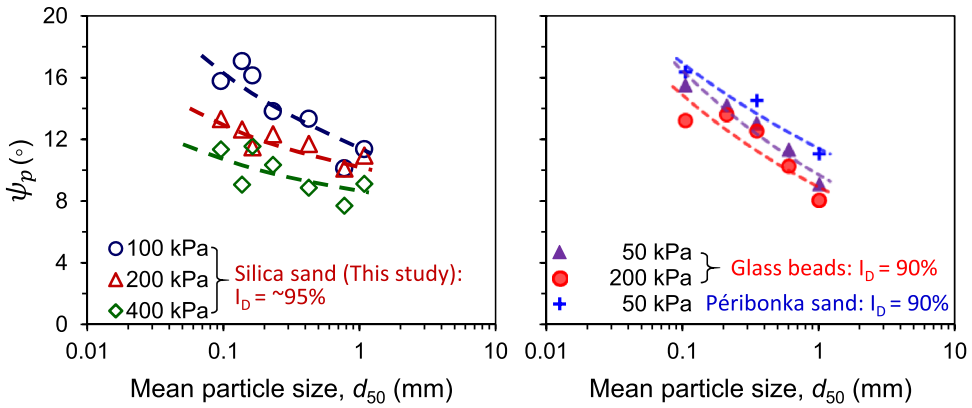

Fig. 12 Influence of particle size and confining stress on dilation angle ψ_p for silica sand, glass beads, and Péribonka sand

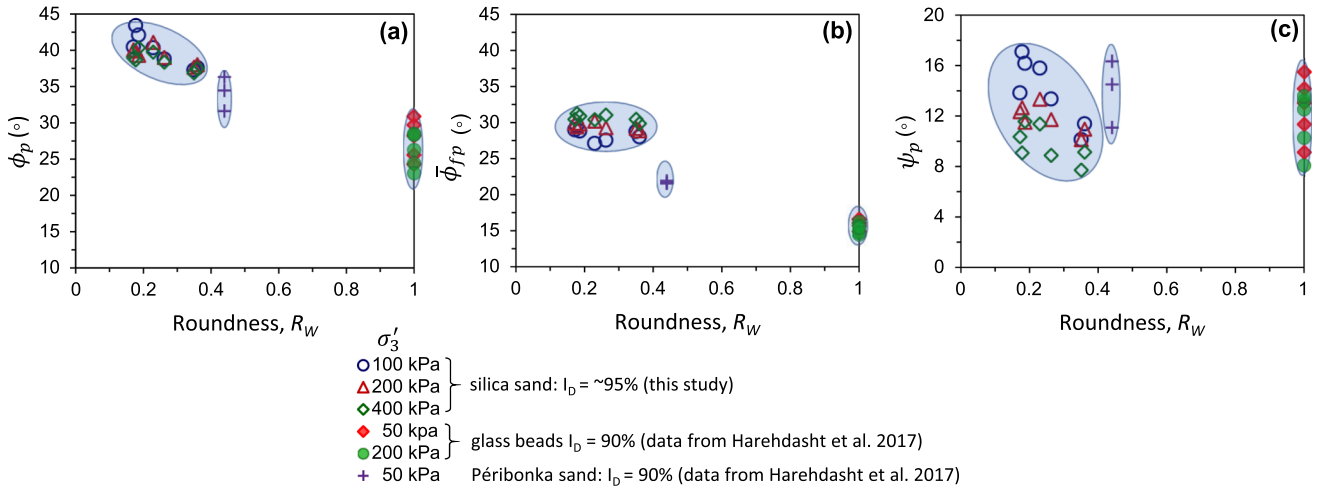

Fig. 13 Influence of particle roundness on peak friction angle ϕ_p, equivalent peak friction angle $\overline{\phi}_{fp}$, and peak dilation angle ψ_p

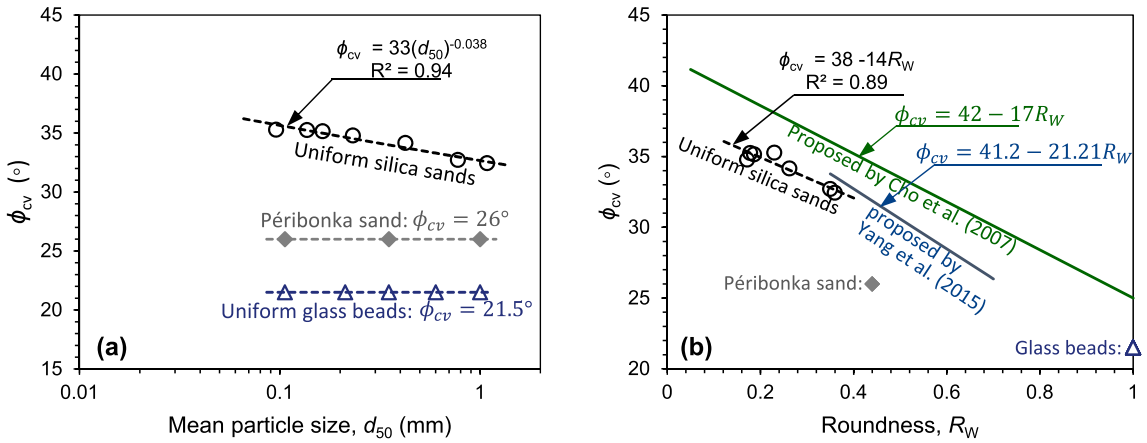

Fig.14 Critical state friction angle ϕ_{cv} versus (a) mean particle size and (b) particle roundness

5.2.2 Influence of particle roundness

In order to assess the influence of particle roundness, we plotted the values of $\overline{\phi}_{fp}$, ϕ_p, and ψ_p versus particle roundness for silica sand, glass beads, and Péribonka sand in Fig. 13. Péribonka sand was considered to be sub-rounded with an average particle roundness of 0.44 and the particle roundness for glass beads is near to 1. The range of particle size for the three materials is almost the same

(0.1 mm-1 mm). The data plotted in Fig. 13 are grouped for three materials. Thus, from the dimension and distribution of the three data groups, the influence of roundness can be assessed.

As shown in Fig. 13, particle roundness has significant influence on ϕ_p, which decreases with an increase in particle roundness. The influence of particle roundness on $\overline{\phi}_{fp}$ is less significant, and the influence of particle roundness on ψ_p is insignificant.

5.3 Critical state friction angle

5.3.1 Influence of particle roundness

The dependence of ϕ_{cv} on particle roundness of sand has been found from the experiments by many investigators [12, 18–20]. In our tests on silica sands, ϕ_{cv} versus particle roundness is shown in Fig. 14b, which shows a strong correlation between ϕ_{cv} and particle roundness (R^2 = 0.89). The regressed relationship is given by

$$\phi_{cv} = 38 - 14R_W \tag{7}$$

As shown in Fig. 14b, the correlation between ϕ_{cv} and particle roundness has the similar trend with that obtained from other types of sands by Cho et al. [18] and with that obtained from Fujian sand mixtures by Yang and Luo [19]. For comparison, the experimental data for Péribonka sand and for glass beads are also plotted on Fig. 14b represented by two points. It shows a general decreasing trend of ϕ_{cv} with an increase in particle roundness.

5.3.2 Influence of particle size

On the other hand, the correlation between ϕ_{cv} and particle size has scarcely reported for sands. Figure 14a shows the influence of particle size on ϕ_{cv} for silica sand, Péribonka sand and glass beads. It is noticed that the measured values of ϕ_{cv} for both glass beads and for Péribonka Sand [1] are independent of particle size as shown in Fig. 14a. In contrast, our tested results showed that the measured value of ϕ_{cv} for silica sand has a strong correlation with particle size (R^2 = 0.94).

The results shown in Fig. 14a reveal that the value of ϕ_{cv} is independent of particle size for glass beads and Péribonka sand. Thus, it is reasonable to expect that the particle size dependence of ϕ_{cv} for silica sand is attributed to the particle roundness effect, since the particle roundness and particle size have a strong correlation for silica sand. This apparent particle size dependence of the value ϕ_{cv} is typical for fluvial sand, which would lead to a different particle size effect on stress–dilatancy relation from that of glass beads.

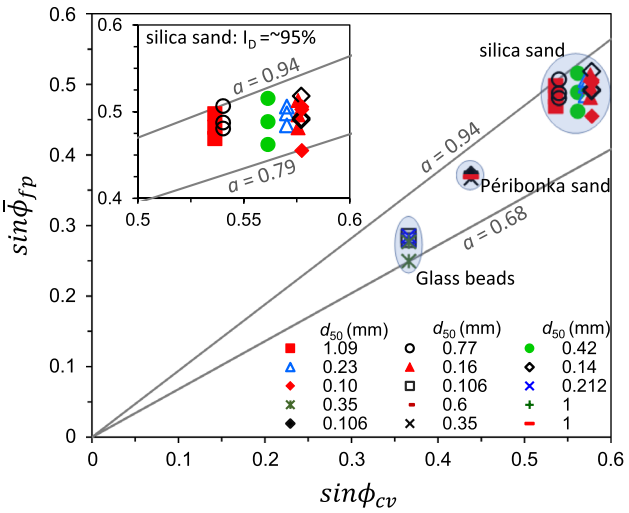

Fig. 15 The relationship between $\sin\phi_{cv}$ and $\sin\overline{\phi}_{fp}$ for glass beads, Péribonka sand, and silica sand under different confining stresses

6 Stress–dilatancy relation

Due to the size-roundness correlation of silica sand, in this section, we investigate the effects of both particle size and particle roundness on stress–dilatancy relations of silica sand, glass beads and Péribonka sand.

6.1 Rowe's stress–dilatancy relation

At peak state, for the Rowe's stress–dilatancy relation in Eq. (3), $\phi_m = \phi_p$, $\overline{\phi}_f = \overline{\phi}_{fp}$, $\psi = \psi_p$. Then, Eq. (3) becomes

$$\sin\phi_p = \frac{\sin\psi_p + \sin\overline{\phi}_{fp}}{1 + \sin\psi_p \sin\overline{\phi}_{fp}} \tag{8}$$

This equation couples the peak dilatancy ψ_p to the peak strength ϕ_p. It can be seen from Fig. 9 that the value of $\overline{\phi}_{fp}$ is in the range between ϕ_μ and ϕ_{cv}. For convenience, Wan and Guo [6] express $\overline{\phi}_{fp}$ in terms of ϕ_{cv} as

$$\sin\overline{\phi}_{fp} = a\sin\phi_{cv} \tag{9}$$

where a is a parameter between 0 and 1. The value of a can be interpreted from experimental results. Figure 15 shows a plot of $\sin\phi_{cv}$ versus $\sin\overline{\phi}_{fp}$ for the three types of materials: glass beads, silica sand and Péribonkas sand. The range of "a" is between 0.68 and 0.94 as shown in Fig. 15. The sub-figure shows that the range is 0.79–0.94 for silica sand.

The measured values of $\sin\phi_{cv}$ and $\sin\overline{\phi}_{fp}$ are plotted in Fig. 16 for silica sand, glass beads and Péribonka sand, in which, the data of glass beads and Péribonka sand were extracted from Harehdasht et al. [1]. As shown in Fig. 16,

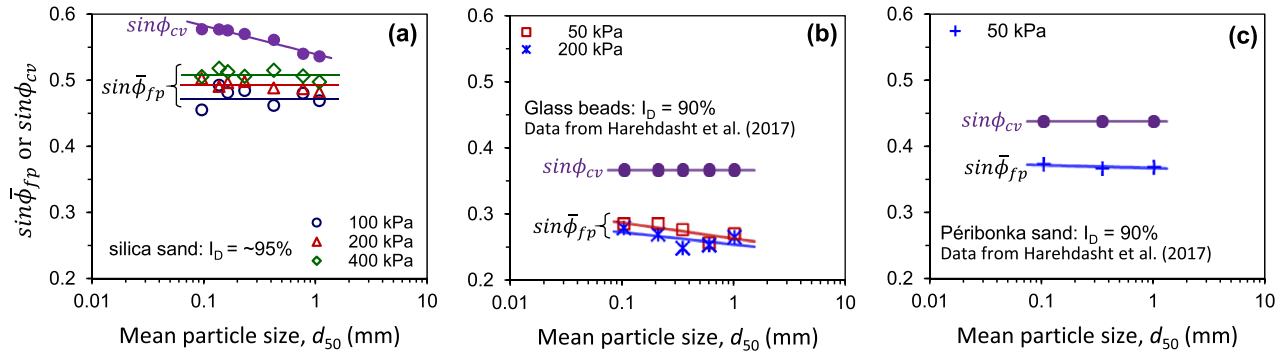

Fig. 16 The equivalent friction angle at peak $\bar{\phi}_{fp}$ or the critical state friction angle ϕ_{cv} versus mean particle size

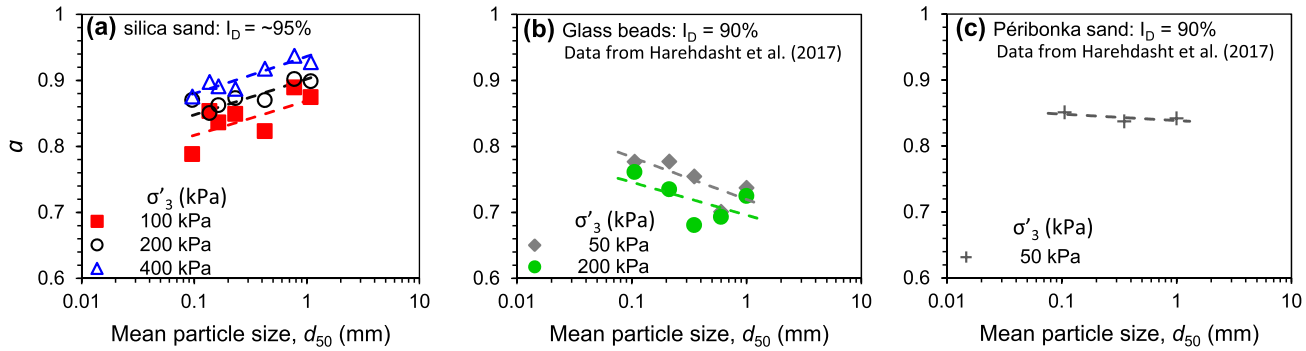

Fig. 17 Particle size effect on the value of parameter a for glass beads, Péribonka sand, and silica sand under different confining stresses

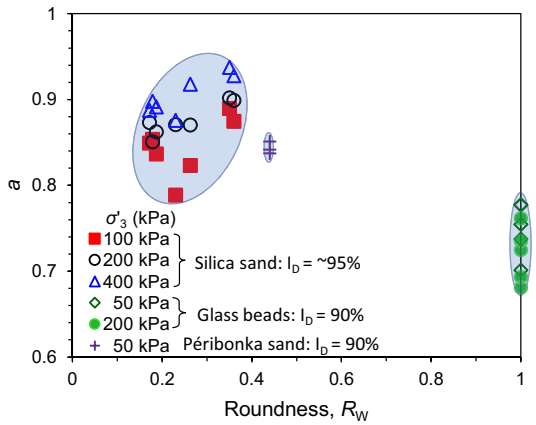

Fig. 18 Particle roundness effect on the value of parameter a for glass beads, Péribonka sand, and silica sand under different confining stresses

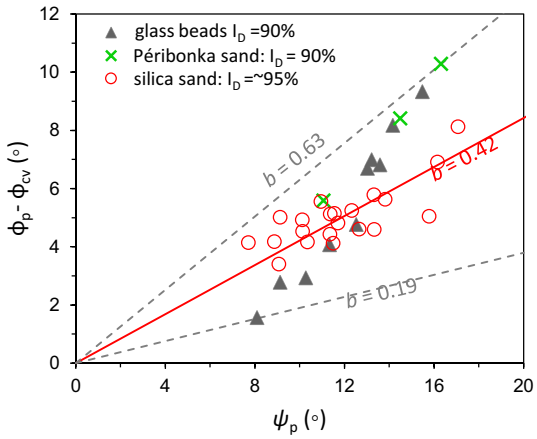

Fig. 19 The overall relationship between $(\phi_p - \phi_{cv})$ and ψ_p for silica sand, Péribonka sand, and glass beads

for Péribonka sand, the curves of $\sin\phi_{cv}$ and $\sin\bar{\phi}_{fp}$ are two parallel lines. For silica sand, the curves of $\sin\phi_{cv}$ and $\sin\bar{\phi}_{fp}$ are two converge lines, i.e., the difference of the two values are becoming smaller as particle size increases. But for glass beads, the curves of $\sin\phi_{cv}$ and $\sin\bar{\phi}_{fp}$ are two diverge lines, i.e., the difference of the two values are becoming larger as particle size increases. These features make the different patterns of parameter a varying with particle sizes between silica sand and glass beads or Péribonka sand.

Base on the measured $\sin\phi_{cv}$ and $\sin\bar{\phi}_{fp}$, the values of a are calculated and plotted in Fig. 17 for silica sand, glass beads and for Péribonka sand. For Péribonka sand, the value of a is nearly a constant with respect to particle size. For silica sand, the value of a increases with particle size. This trend is contrary to the results of glass beads. The

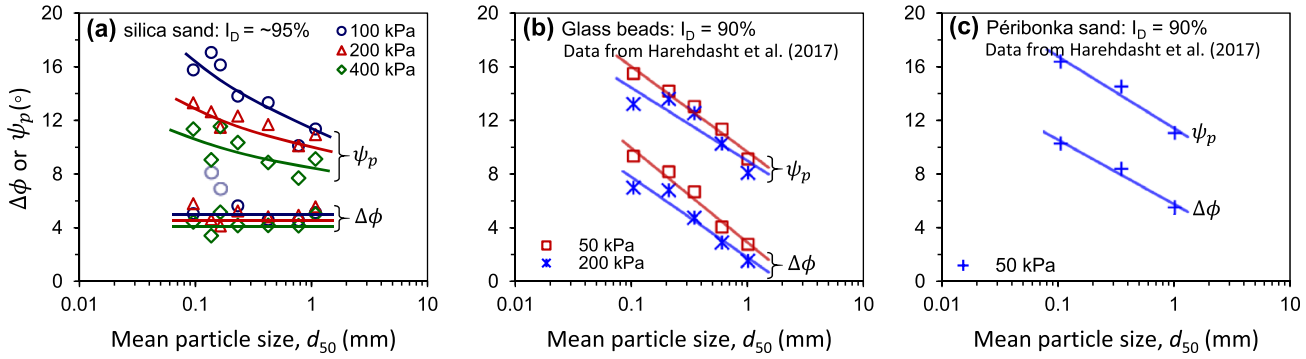

Fig. 20 Particle size effect on $\Delta\phi$ or ψ_p for glass beads, Péribonka sand, and glass beads under different confining stresses

opposite trends can be explained by the curves of $\sin\phi_{cv}$ and $\sin\overline{\phi}_{fp}$, shown in Fig. 16.

Figure 18 shows the value of a influenced by particle roundness for silica sand, Péribonka sand and glass beads. The trend shows that parameter a decreases with an increase in roundness.

6.2 Bolton's stress–dilatancy relation

Bolton's stress–dilatancy relation [17] is an alternative of Rowe's stress–dilatancy relation [2].

$$\Delta\phi = \phi_p - \phi_{cv} = b\psi_p \tag{10}$$

where b is a parameter implying the contribution of dilatancy to the peak strength.

Figure 19 shows a plot of ψ_p versus $\phi_p - \phi_{cv}$ for glass beads, Péribonka sand and silica sand. The range of "b" is between 0.19 and 0.63 as shown in Fig. 19. The value of b from the 21 silica sand test results is plotted in Fig. 19 with an averaged value of b = 0.42, which is close to b = 0.48 in the Bolton's equation for clean sands under triaxial compression condition [17].

According to Eq. (10), the parameter b is influenced by the values of ϕ_p, ϕ_{cv} and ψ_p. Figure 20 shows the $\Delta\phi$ and ψ_p versus particle size for silica sand, glass beads, and

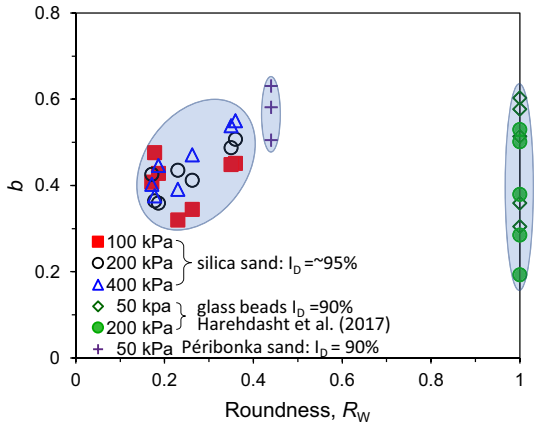

Fig. 22 Influence of particle roundness on parameter b

Péribonka sand. Due to the different behavior of ϕ_p and ϕ_{cv} of three types of materials, $\Delta\phi = \phi_p - \phi_{cv}$ decreases with particle size for glass beads and Péribonka sand, but is nearly independent of particle size for silica sand.

For Péribonka sand, the curves of $\Delta\phi$ and ψ_p are two nearly parallel lines. For glass beads, the two lines are diverged. For silica sand, however, the two lines are converged.

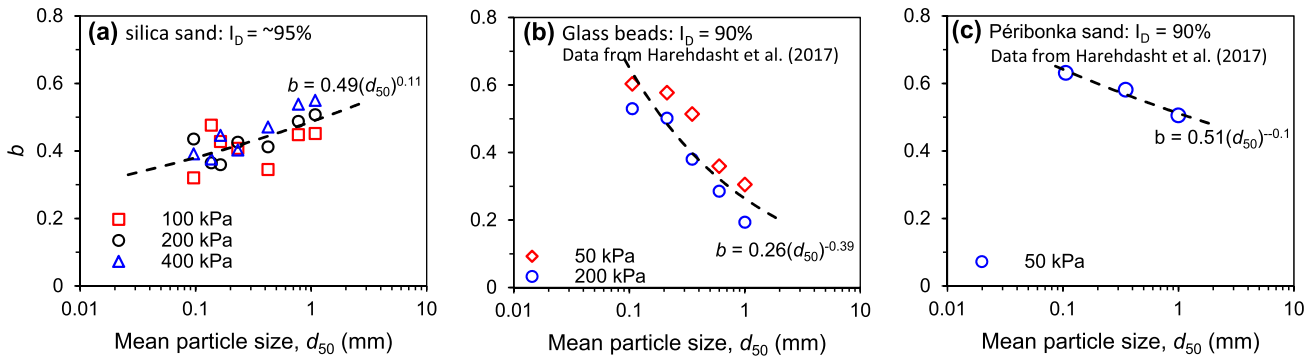

Fig. 21 Particle size effect on the value of parameter a for glass beads, Péribonka sand, and silica sand under different confining stresses

From the behavior of $\Delta\phi$ and ψ_p shown in Fig. 20, the value of $b = (\phi_p - \phi_{cv})/\psi_p$ are computed and plotted in Fig. 21 with respect to particle size for silica sand, glass beads, and Péribonka sand. The parameter b decreases with particle size for glass beads and Péribonka sand, but increases with particle size for silica sand. The opposite trends of b between silica sands and glass beads or Péribonka sand, are mainly caused by the different patterns of $\Delta\phi$ and ψ_p shown in Fig. 20

The effect of particle roundness on the value of b for the three types of materials is shown in Fig. 22. Opposite to Fig. 18 for the parameter a, Fig. 22 does not show a clear trend of "b" versus particle roundness.

7 The underlying particle-level mechanism for influences of particle size and confining stress

The experimental results in this study have confirmed that particle size has significant influence on the peak friction and dilation angles, but has no effect on critical state friction angle. The underlying mechanism is not clear for the effect of particle size.

Harehdasht et al. [1] attributed it to the difference in stress chains, which are highly concentrated for a small particle sample and are diffused for a large particle sample. Herein, we aim to explain the underlying mechanism for the effect of particle size from another perspective.

The deformation of a soil sample is a transition process from homogeneous strain field to a highly non-uniform strain field [50]. The underlying particle-level mechanism for the soil deformation can be described as the buildup of particle columns during the hardening process and the collapse of particle columns during the softening process [11, 51].

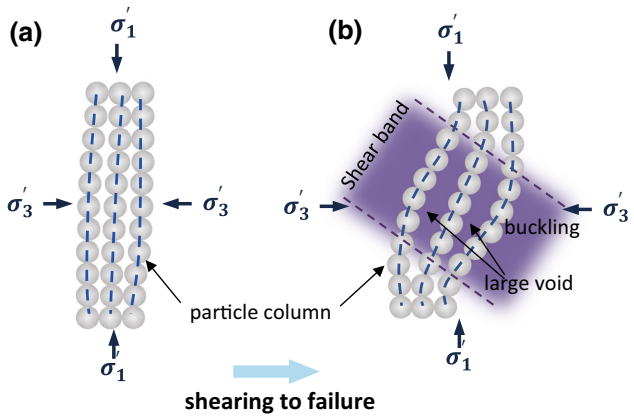

Fig. 23 A schematic diagram illustrating the mechanism for dilatancy: **a** buildup of particle columns and **b** buckling particle columns

According to Iwashita and Oda [51], in the hardening process up to failure, particles are rearranged in chains to form particle columns aligned in the direction of the major principal stress axis. The applied load is mainly transmitted through them in the form of force chains, as shown in Fig. 23a.

During the loading process, the pre-existing contacts are lost in the minor principal stress direction, but new contacts are formed in the major principal stress direction. Consequently, the particle columns bend, and elongated voids are generated between neighboring columns. This is the mechanism causing dilatancy before failure.

Due to the formation of particle columns and the elongated void parallel to the major principal stress direction, the packing structure becomes highly anisotropic as load increases. Such anisotropic structure becomes gradually unstable as a result of the loss of surrounding contact points. Finally, the particle columns are collapsed via buckling, as shown in Fig. 23b. The buckling is associated with particle rotation and causes the growth of voids between buckling columns.

The number of buckled columns increases during the loading process, eventually, the sample cannot carry further load, i.e., the peak stress is reached. The further axial strain deformation leads to a softening of the sample after the peak stress failure.

After peak stress, a new packing structure is re-constructed during the softening process. The continuing buckling of particle columns is gradually concentrated in a narrow shear band, which causes rotation of particles and the growth of voids in the shear band. Finally, the structure reaches a dynamically stable condition at the critical state. At the critical state, buildup and collapse of particle columns keep equilibrium within persistent shear bands. The dilatancy is balanced with the contraction so that the overall volumetric strain remains unchanged, resulting in a constant void ratio.

The effects of particle size can be explained by the mechanism of particle column buckling. The particle columns formed in a small-particle sample are slenderer than those formed in a large-particle sample. The slender particle columns are easier to bend/buckle. Thus, it requires smaller axial strain to buckle the slender particle columns in the soil sample.

For a given axial strain increment, there are more bending of particle columns in a small-particle sample. Thus, the generated elongated void between two particle columns results in a higher void ratio and consequently a higher dilatancy rate. The higher dilatancy rate makes the packing structure more anisotropic and capable of carrying higher vertical load than that of a large-particle sample. Thus, the small-particle sample would result in a higher peak friction angle ϕ_p and higher peak dilation angle ψ_p.

The critical state friction angle ϕ_{cv}, on the other hand, is not associated with particle column buckling. It is measured under a friction mode of particles at large shear strain. Therefore, particle size has very little effect on the value of ϕ_{cv}.

8 Summary and conclusions

In this paper, the effects of particle size on the shear strength and the stress–dilatancy behavior of sands are assessed through a series of drained triaxial compression tests on dense uniform silica sands. The effects of particle size are analyzed on various aspects of mechanical behavior: the stress–strain response, the shear band formation, the peak-stress axial strain, the peak dilation angle, the peak friction angle, the critical-state friction angle, and the stress–dilatancy equations. The effect of size-roundness correlation of silica sand is also discussed by comparing with experimental results on glass beads and Péribonka sand reported by Harehdasht et al. [1]. Based on this study the major conclusions can be drawn as follows:

(1) Compared to large particle samples, the smaller particle samples are more likely to have visible shear band formation and require a smaller axial strain to reach the peak stress.
(2) Both the peak friction angle ϕ_p and the peak dilation angle ψ_p decrease with an increase in particle size, which confirms the experimental findings reported by Harehdasht et al. [1] on glass beads and Péribonka sand.
(3) The effect of particle size on peak friction angle ϕ_p and peak dilation angle ψ_p can be explained from a perspective of particle column buckling. Since buckling of the particle column is affected by the slenderness of the particle column, thus particle size plays an important role.
(4) Critical state friction angle ϕ_{cv} is independent with particle size as observed in glass beads experiments. For silica sand, the apparent dependence of critical state friction angle ϕ_{cv} on particle size is attributed to the effect of particle roundness which varies with particle size in unison. The dependence of ϕ_{cv} on particle size is a common feature for a fluvial sand.
(5) The observed results on silica sand show an increasing trend with respect to particle size for either the parameter a in Rowe's stress–dilatancy relation or the parameter b in Bolton' stress–dilatancy relation. This trend is opposite to that for Péribonka sand and glass beads. The two opposite trends are mainly caused by the size-roundness correlation of silica sand, which results in a particle size dependent ϕ_{cv} being different from that of glass beads and Péribonka sand.

Appendix A: Sample variability

See Fig. 24.

The effect of sample variability on the stress–strain curves in Fig. 4 is carefully evaluated by repeating several tests under the same testing conditions. A set of typical repeated tests for the uniform sand #50-#80 with a confining pressure of 200 kPa are shown in this Appendix.

Figure 24 shows the stress–strain curves for two different specimens of the uniform sand #50-#80 under the same sample preparation method. The initial void ratios for the two specimens are 0.767 and 0.769. Both specimens were tested in the same triaxial cell under the same confining pressure (200 kPa).

The curves of these two tests are nearly identical before the peak stress. After the peak stress, there is small variation between the curves of the two tests. The variation is likely due to the difference in the locations of strain localization, which was initiated randomly in the two different specimens.

Although the variation is small for the stress–strain curve, we would like to evaluate the possible effect, which

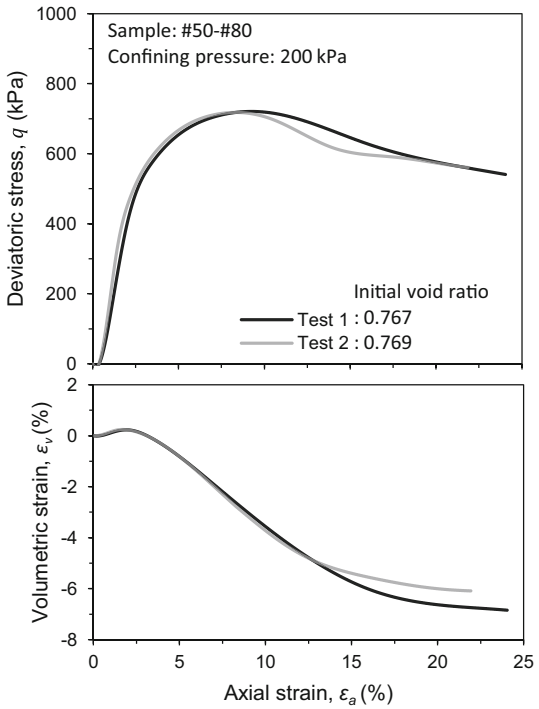

Fig. 24 Experimental results of stress ratio and volumetric strain plotted against axial strain for two specimens of the uniform sand #50-#80 under the same condition

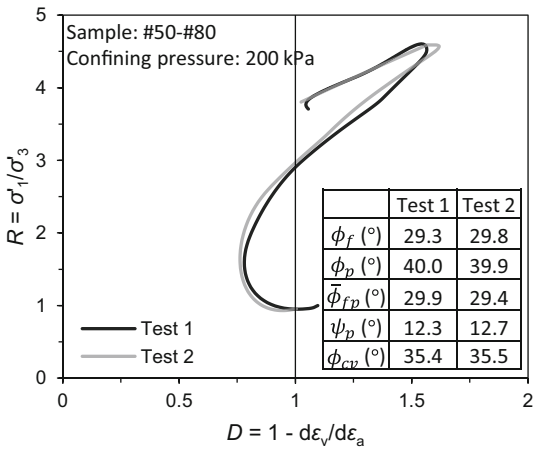

Fig. 25 The stress–dilatancy relations for two specimens of the uniform sand #50-#80 under the same condition

may be caused by this small variation, on various mechanical properties interpreted from the test results, such as peak friction angle, peak dilation angle, and critical-state friction angle.

For this purpose, in Fig. 25, the stress–dilatancy curves is calculated and plotted. Using Fig. 25, the peak friction angle ϕ_p, the friction angle at onset of dilation ϕ_f, the equivalent peak friction angle $\overline{\phi}_{fp}$, and the peak dilation angle ψ_p are computed for the two tests and listed in the figure. The critical state friction angle ϕ_{cv} is computed by Eq. (5) with $T_n = 1$ from each test result. The critical state angle is also listed in Fig. 25. For all computed angles from the stress–strain curves, the difference due to sample variation is less than 0.5 degree, which is acceptable.

Appendix B: Definition of Dilation angle

The expression of dilation angle (ψ) has been proposed by Vermeer and de Borst [35] for triaxial compression and plain strain conditions, which was derived from concepts of plasticity theory. The expression of dilation angle (ψ) is given by:

$$\sin\psi = \frac{-(d\varepsilon_v/d\varepsilon_1)}{2-(d\varepsilon_v/d\varepsilon_1)} \tag{11}$$

In plain strain conditions, Eq. (11) leads to the following expression:

$$\sin\psi = -\frac{(d\varepsilon_1 + d\varepsilon_3)}{(d\varepsilon_1 - d\varepsilon_3)} \tag{12}$$

where $d\varepsilon_1$ and $d\varepsilon_3$ are the principal stain increments and $d\varepsilon_1$ is the axial strain increment $d\varepsilon_a$ in triaxial compression conditions. Equation (11) has been extensively used for calculating the dilation angle of axisymmetric samples [12, 13, 21–23].

An alternative expression of the dilation angle for triaxial compression conditions has been proposed by Vaid and Sasitharan [52] and is given by:

$$\sin\psi = \frac{2}{1-3/(d\varepsilon_v/d\varepsilon_a)} \tag{13}$$

This expression has been used for calculating the dilation angle of axisymmetric samples [1, 53, 54]. This expression was derived from the definition of ψ for plain strain conditions originally introduced by Hansen (1958) given as:

$$\sin\psi = -\frac{d\varepsilon_v}{d\gamma} = -\frac{d\varepsilon_v}{d\varepsilon_1 - d\varepsilon_3} \tag{14}$$

where γ is shear strain.

For plain strain conditions, Eqs. (11) and (14) are identical. However, for triaxial compression conditions, the value of dilation angle (ψ) calculated from Eq. (11) is less than that calculated from Eq. (13) because the definition of $d\gamma$ is different (i.e., $d\gamma = d\varepsilon_1 - 2d\varepsilon_3$ in Eq. (11) while $d\gamma = d\varepsilon_1 - d\varepsilon_3$ in Eq. (13)).

Thus, it is noted that, for plain strain conditions, there is a universal and clear definition of dilation angle. But for triaxial compression conditions, there are two different definitions of dilation angle (Eqs.11 and 13). In this study, the definition of Eq. (11) was used.

Acknowledgement This work was supported by the National Science Foundation of the United States under a research grant (CMMI-1917238). The support is greatly acknowledged.

References

1. Harehdasht SA, Karray M, Hussien MN, Chekired M (2017) Influence of Particle Size and Gradation on the Stress-Dilatancy Behavior of Granular Materials during Drained Triaxial Compression. Int J Geomech 17:04017077. https://doi.org/10.1061/(ASCE)GM.1943-5622.0000951
2. Rowe PW (1962) The stress dilatancy relation for static equilibrium of an assembly of particles in contact. Proceed R Soc 269A:500–527
3. De Josselin De Jong G (1976) Rowe's stress–dilatancy relation based on friction. Geotechnique 26:527–534
4. Hughes JMO, Wroth CP, Windle D (1977) Pressuremeter test in sands. Geotechnique 27:455–477
5. Wan RG, Guo PJ (1998) A simple constitutive model for granular soils: Modified stress-dilatancy approach. Comput Geotech 22:109–133
6. Wan RG, Guo PJ (1999) A pressure and density dependent dilatancy model for granular materials. Soils Found 39:1–11
7. Zhang J, Salgado R (2010) Stress-dilatancy Relation for Mohr-Coulomb Soils Following a Non-Associated Flow Rule. Geotechnique 60:223–226. https://doi.org/10.1680/geot.8.T.039
8. Vesic AS, Clough GW (1968) Behavior of granular materials under high stresses. J Soil Mech Found Div 94:661–688

9. Billiam J (1972) Some aspects of the behaviour of granular materials at high pressures. In: Parry RHG (ed) Stress. Behav. Soils, Foulis, London, UK, pp 69–80
10. Bishop AW (1972) Shear strength parameters for undisturbed and remoulded soils specimens. In: Parry RHG (ed) Stress. Behav. Soils, Foulis, London, UK, pp 3–58
11. Oda M (1972) Initial fabrics and their relations to mechanical properties of granular materials. Soils Found 12:17–36
12. Alshibli KA, Cil MB (2018) Influence of particle morphology on the friction and dilatancy of sand. J Geotech Geoenviron Eng 144:1–12. https://doi.org/10.1061/(ASCE)GT.1943-5606.0001841
13. Xiao Y, Long L, Evans TM et al (2019) Effect of particle shape on stress-dilatancy responses of medium-dense sands. J Geotech Geoenviron Eng 145:1–15. https://doi.org/10.1061/(ASCE)GT.1943-5606.0001994
14. Xiao Y, Xiang J, Liu H, Ma Q (2017) Strength-dilatancy relation of sand containing non-plastic fines. Géotechnique Lett 7:204–210. https://doi.org/10.1680/jgele.16.00144
15. Guo P, Su X (2007) Shear strength, interparticle locking, and dilatancy of granular materials. Can Geotech J 44:579–591. https://doi.org/10.1139/T07-010
16. Guida G, Sebastiani D, Casini F, Miliziano S (2020) Grain morphology and strength dilatancy of sands. Géotechnique Lett 9:245–253. https://doi.org/10.1680/jgele.18.00199
17. Bolton MD (1986) The strength and dilatancy of sands. Géotechnique 36:65–78. https://doi.org/10.1680/geot.1986.36.1.65
18. Cho G-C, Dodds J, Santamarina JC (2006) Particle Shape Effects on Packing Density, Stiffness, and Strength: Natural and Crushed Sands. J Geotech Geoenviron Eng 132:591–602. https://doi.org/10.1061/(ASCE)1090-0241(2006)132:5(591)
19. Yang J, Luo XD (2015) Exploring the relationship between critical state and particle shape for granular materials. J Mech Phys Solids 84:196–213. https://doi.org/10.1016/j.jmps.2015.08.001
20. Altuhafi FN, Coop MR, Georgiannou VN (2016) Effect of Particle Shape on the Mechanical Behavior of Natural Sands. J Geotech Geoenviron Eng 142:04016071. https://doi.org/10.1061/(ASCE)GT.1943-5606.0001569
21. Salgado R, Bandini P, Karim A (2000) Shear Strength and Stiffness of Silty Sand. J Geotech Geoenviron Eng 126:451–462. https://doi.org/10.1061/(ASCE)1090-0241(2000)126:5(451)
22. Esposito MP, Andrus RD (2017) Peak Shear Strength and Dilatancy of a Pleistocene Age Sand. J Geotech Geoenviron Eng 143:04016079. https://doi.org/10.1061/(ASCE)GT.1943-5606.0001582
23. Cinicioglu O, Abadkon A (2015) Dilatancy and Friction Angles Based on In Situ Soil Conditions. J Geotech Geoenviron Eng 141:06014019. https://doi.org/10.1061/(ASCE)GT.1943-5606.0001272
24. Azéma E, Linero S, Estrada N, Lizcano A (2017) Shear strength and microstructure of polydisperse packings: The effect of size span and shape of particle size distribution. Phys Rev E 96:022902. https://doi.org/10.1103/PhysRevE.96.022902
25. Nguyen D-H, Azéma É, Sornay P, Radjaï F (2015) Effects of shape and size polydispersity on strength properties of granular materials. Phys Rev E 91:032203. https://doi.org/10.1103/PhysRevE.91.032203
26. Estrada N (2016) Effects of grain size distribution on the packing fraction and shear strength of frictionless disk packings. Phys Rev E 94:062903. https://doi.org/10.1103/PhysRevE.94.062903
27. Frossard E, Dano C, Hu W, Hicher P-Y (2012) Rockfill shear strength evaluation: a rational method based on size effects. Géotechnique 62:415–427. https://doi.org/10.1680/geot.10.P.079
28. Varadarajan A, Sharma KG, Venkatachalam K, Gupta AK (2003) Testing and Modeling Two Rockfill Materials. J Geotech Geoenvironmental Eng 129:206–218. https://doi.org/10.1061/(ASCE)1090-0241(2003)129:3(206)
29. Wadell H (1935) Volume, Shape, and Roundness of Quartz Particles. J Geol 43:250–280
30. ASTM D4253-00 (2006) Standard test methods for maximum index density and unit weight of soils using a vibratory table. In: Annu. B. ASTM Stand. ASTM International, West Conshohocken, PA, pp 1–15
31. ASTM D4254-00 (2006) Standard Test Methods for Minimum Index Density and Unit Weight of Soils and Calculation of Relative Density. In: Annu. B. ASTM Stand. ASTM International, West Conshohocken, PA, pp 1–9
32. Alshibli1 KA, Sture S (2000) Shear band formation in plane strain experiments of sand. J Geotech Geoenvironmental Eng 126:495–503 https://doi.org/10.1061/(ASCE)1090-0241(2000)126:6(495)
33. Viggiani G, Kuentz M, Desrues J (2001) An experimental investigation of the relationships between grain size distribution and shear banding in sand. In: Diebels S, Ehlers W et al (eds) Vermeer PA. Contin. discontinuous Model. cohesive-frictional Mater. Springer, New York, USA, pp 111–127
34. Sadrekarimi A, Olson SM (2010) Shear band formation observed in ring shear tests on sandy soils. J Geotech Geoenvironmental Eng 136:366–375. https://doi.org/10.1061/(ASCE)GT.1943-5606.0000220
35. Vermeer PA, de Borst R (1984) Non-associated plasticity for soils, concrete and rock. HERON 29:1–64
36. King GJW, Dickin E (1970) Comparison of stress-dilatancy theories. J Soil Mech Found Div 96(SM5):1697–1714
37. Schofield AN, Wroth CP (1968) Critical state soil mechanics. McGraw-Hill, Maidenhead, England
38. Nova R (1982) A constitutive model under monotonic and cyclic loading. In: Pande G, Zienkiewicz OC (Eds.), Soil Mechanics — Transient and Cyclic Loads. John Wiley & Sons Ltd., New York, USA, pp 343–373
39. Russell RD (1937) Mineral composition of mississippi river sands. Bull Geol Soc Am 48:1307–1348
40. Balazs RJ, Klein GD (1972) Roundness-mineralogical relations of some intertidal sands. J Sediment Res 42:425–433. https://doi.org/10.1306/74D72577-2B21-11D7-8648000102C1865D
41. Inman DL (1953) Areal and seasonal variations in beach and nearshore sediments at La Jolla, California.
42. Pettijohn FJ, Lundahl AC (1943) Shape and roundness of Lake Erie beach sands. J Sediment Petrol 13:69–78. https://doi.org/10.1306/D426919D-2B26-11D7-8648000102C1865D
43. Inman DL, Ewing GC, Corliss JB (1966) Coastal Sand Dunes Of guerrero Negro, baja Caolifornia, Mexico. GSA Bull 77:787–802
44. Ramez MRH, Mosalamy FH (1969) the Deformed Nature of Various Size Fractions in Some Clastic Sands. J Sediment Petrol Artic 39:1182–1187
45. Youd TL (1973) Factors Controlling Maximum and Minimum Densities of Sands. In: Eval. Relat. Density its Role Geotech. Proj. Involv. Cohesionless Soils,STP 523. ASTM International, West Conshohocken, PA, pp 98–112
46. Edil TB, Krizek RJ, Zelasko JS (1975) Effect of grain characteristics on packing of sands. Proc. Istanbul Conf Soil Mech Found Eng. Istanbul Technical University, Istanbul, Turkey, pp 46–54
47. Norris GM (1977) The drained shear strength of uniform quartz sand as related to particle size and natural variation in particle shape and surface roughness. Ph.D. thesis, University of California, Berkeley

48. Thomann TG (1990) Stiffness and strength changes in cohensionless soils due to stress history and dynamic disturbance. University of Michigan, Ann Arbor, Mich
49. Chang CS, Meidani M, Deng Y (2018) Role of morphologic indices on the variation of limiting void ratios for uniform sands. Géotechnique Lett 8:248–255. https://doi.org/10.1680/jgele.18.00087
50. Harris WW, Viggiani G, Mooney MA, Finno RJ (1995) Use of Stereophotogrammetry to Analyze the Development of Shear Bands in Sand. Geotech Test J 18:405–420
51. Iwashita K, Oda M (2000) Micro-deformation mechanism of shear banding process based on modified distinct element method. Powder Technol 109:192–205
52. Vaid YP, Sasitharan S (1992) The strength and dilatancy of sand. Can Geotech J 29:522–526. https://doi.org/10.1139/t92-058
53. Chen X, Zhang J (2016) Effect of clay invasion on shear behavior and dilatancy of unbound aggregate subbase. Transp Geotech 6:16–25. https://doi.org/10.1016/j.trgeo.2015.12.001
54. Frydman S, Talesnick M, Nawatha H, Schwartz K (2007) Stress-dilation of undisturbed sand samples in drained and undrained triaxial shear. Soils Found 47:27–32. 0.3208/sandf.47.27
55. Hansen B (1958) Liner ruptures regarded as narrow rupture zones - Basic equations based on kinematic considerations. In: Proc. 10th Eur. Conf. Earth Press. Probl. Brussels, Belgium, pp 39–48
56. Pettijohn FJ (1957) Sedimentary rocks. Harper, New York, USA